

NUFFT-ACCELERATED PLANE-POLAR (ALSO PHASE-LESS) NEAR-FIELD/FAR-FIELD TRANSFORMATION

Amedeo Capozzoli*, Claudio Curcio, and Angelo Liseno

Dipartimento di Ingegneria Biomedica, Elettronica e delle Telecomunicazioni, Università di Napoli Federico II, via Claudio 21, Napoli I 80125, Italy

Abstract—The paper introduces the use of Non-Uniform Fast Fourier Transform (NUFFT) routines in “complex” (i.e., amplitude and phase) and phaseless Near-Field/Far-Field transformations. The use of those routines results computationally very convenient when non-regular field sampling prevents the use of standard FFTs. The attention is focused on a plane-polar acquisition geometry. Numerical and experimental results show the effectiveness of the developed algorithms.

1. INTRODUCTION

In near-field (NF) antenna characterization [1], two relevant topics regard the reduction of the NF scanning time and the fast computation of the far-field (FF) from the acquired NF samples.

Concerning the first topic, several techniques have been proposed in various scanning geometries, as the Cartesian [2], the plane-polar [3, 4], the planar wide-mesh [5], the spiral [6], the rectangular-spiral [7], and the helicoidal [4] ones. The Authors have contributed in this framework by an advanced non-uniform sampling technique [8], capable to significantly reducing the acquisition time and the ill-conditioning as compared to other non-uniform samplings, and which has been also applied to the cases of a plane-polar [9] and “quasi-raster” [10] configurations.

Regarding the second topic, when complex measurements of the NF are available on a regular, Cartesian grid, the field spectrum calculation requires a simple Fourier transform operation, which can be performed by a standard Fast Fourier Transform (FFT) routine having a very convenient asymptotic computational complexity growing as

Received 15 September 2012, Accepted 9 November 2012, Scheduled 14 November 2012

* Corresponding author: Amedeo Capozzoli (a.capozzoli@unina.it).

$N \log N$, where N is the overall number of samples [1]. However, when non-uniform grids are involved, standard FFTs do not apply anymore. Due to the computational convenience of the FFT, a popular way to carry out the NFFF transformation is to perform an interpolation stage prior to the FFT [3, 11, 12], instead of proceeding by a more computationally demanding matrix-vector multiplication [13]. This establishes a trade-off between accuracy and computational complexity [14, 15]. Such a trade-off becomes more critical in the case of algorithms relying on phaseless data which are based on an iterative optimization process so that, at each iteration step, they necessitate evaluating the spectrum from estimates of the NF on non-uniform lattices or calculating the NF on non-uniform grids from estimates of the spectrum. In the last years, Non-Uniform FFT (NUFFT) algorithms [16, 17] have been developed enabling to evaluate Fourier transforms from non-uniform grids to uniform ones (Non-Equispaced Data NED-NUFFT) [16, 17], from uniform grids to non-uniform ones (Non-Equispaced Results NER-NUFFT) [16, 17] and from non-uniform grids to non-uniform ones (type-3 NUFFT) [18]. Such algorithms enable to accurately performing the interpolation stage in a computationally convenient way, so that their burden is proportional to that of a standard FFT. Furthermore, NUFFTs can be made available as library routines to make more friendly their usage and, accordingly, their exploitation in NFFF transformations, as well as other application fields [19].

The topic of this paper is a computational one and regards the fast evaluation of the FF from non-uniform NF samples. Our purpose is to show how NUFFT routines can be conveniently employed in NF characterization algorithms exploiting non-uniform samples, operating both with complex or phaseless data. To this end, we focus the attention on the conventional version of the plane-polar (complex or phaseless) acquisition geometry, with a sampling step of $\lambda/2$ or $\lambda/4$ for the complex or phaseless case, respectively, in both the radial and angular directions [20], λ being the wavelength. Although non-optimal from the point of view of the scanning duration, it clearly enables to highlight the benefits of using the NUFFT in a simple case and without resorting to more involved, time consuming interpolators. Numerical and experimental results show the computational convenience and the accuracy of the proposed technique.

The paper is organized as follows. In Sections 2 and 3, the adopted complex and phaseless NFFF transformations in a plane-polar scanning geometry are recalled. It is also shown how propagation from scanning planes to far-field (FF) and backpropagation from FF to scanning planes can be performed by NED and NER NUFFT routines,

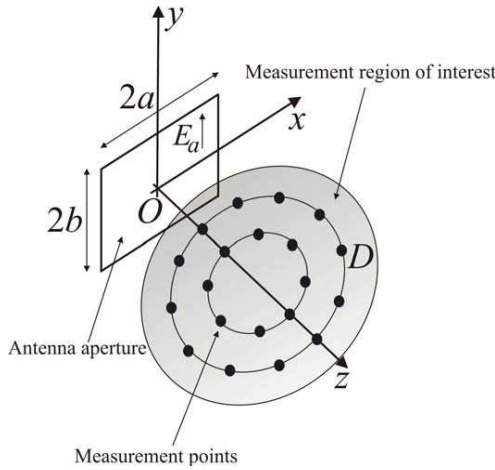


Figure 1. Geometry of the complex NFFF transformation problem.

respectively. In Section 4, the rationales of NED and NER NUFFT routines are briefly sketched. Section 5 contains the numerical and experimental results proving the performance of the approach and, finally, in Section 6 the conclusions are drawn.

2. “COMPLEX” NFFF TRANSFORMATION

Let us thus consider a rectangular aperture, $2a \times 2b$ sized and centered in the $Oxyz$ reference system, with a linearly polarized aperture field $\underline{E}_a = E_a \hat{i}_y$, where \hat{i}_y is the unit vector along the y -axis (see Figure 1), so that, without any loss of generality, a scalar NFFF transformation problem can be faced. The probe is assumed to be electrically small, so that probe correction can be assumed to be irrelevant [20], linearly polarized, y -oriented and co-rotated with the AUT [20] so that only the y component E of the radiated NF over the region of interest D located on the plane $z = d$ (Figure 1) is measured. We explicitly mention that more general configurations can be easily afforded.

The samples of E are acquired at the locations $(\rho_m \cos \phi_{mn}, \rho_m \sin \phi_{mn})$ of the $z = d$ plane, according to the plane-polar scanning geometry [20], where ρ and ϕ are the radial and angular coordinates of such a plane. For the sake of simplicity, but without any loss in generality, the sampling step $\Delta\rho_m$ in ρ is chosen to be $\lambda/2$, while the sampling step $\Delta\phi_m$ in ϕ is constant on each ring (but changes from ring to ring) and chosen so that a sampling step of approximately $\lambda/2$ is obtained also angularly. In other words, for the m -th ring (having

radius ρ_m), the angular sampling step is $\Delta\phi_m = \lambda/(2\rho_m)$.

In this paper we refer to a standard NFFF transformation, different from the technique proposed in [9] and based on the use of a Singular Value Decomposition approach, but improved with a filtering which exploits a priori information on shape and size of the aperture.

Beginning with the standard NFFF transformation [1], we recall that it amounts at estimating the y component $\hat{E}(u, v)$ of the Plane Wave Spectrum (PWS) from the samples of $E(\rho_m \cos \phi_{mn}, \rho_m \sin \phi_{mn})$ as

$$\begin{aligned} \hat{E}(u_p, v_q) &= e^{jw_{pq}d} \iint_D E(x, y, d) e^{j[u_p x + v_q y]} dD \simeq e^{jw_{pq}d} \\ &\times \sum_{m,n} \rho_m \Delta\rho_m \Delta\phi_m E(\rho_m \cos \phi_{mn}, \rho_m \sin \phi_{mn}) \\ &e^{j[u_p \rho_m \cos \phi_{mn} + v_q \rho_m \sin \phi_{mn}]} \end{aligned} \quad (1)$$

where (u_p, v_q) are the $N \times N$ spectral locations of interest, $w_{pq} = \sqrt{\beta^2 - u_p^2 - v_q^2}$, and $\beta = 2\pi/\lambda$ is the wavenumber. After that, from the PWS, the FF is retrieved.

By considering the index correspondence $k = k(m, n)$, and by letting

$$\begin{cases} x_k = \rho_m \cos \phi_{mn} \\ y_k = \rho_m \sin \phi_{mn} \\ f_k = \rho_m \Delta\rho_m \Delta\phi_m E(\rho_m \cos \phi_{mn}, \rho_m \sin \phi_{mn}) \end{cases}, \quad (2)$$

and

$$\begin{cases} u_p = p \frac{2\beta}{N} & p = -\frac{N}{2}, \dots, \frac{N}{2} \\ v_q = q \frac{2\beta}{N} & q = -\frac{N}{2}, \dots, \frac{N}{2} \end{cases}, \quad (3)$$

then Eq. (1) can be rewritten in the form of a Non-Uniform DFT (NUDFT) of the NED type as [16, 17]

$$\hat{E}(u_p, v_q) = e^{jw_{pq}d} \sum_{k=1}^K f_k e^{j2\pi \left[\frac{p}{N} \left(\frac{2x_k}{\lambda} \right) + \frac{q}{N} \left(\frac{2y_k}{\lambda} \right) \right]}. \quad (4)$$

At variance with a standard DFT, the NED-NUDFT transforms non-equispaced data into an equally-spaced array and, as it will be seen in the next Section, can be conveniently calculated by a NED-NUFFT. Accordingly, NED-NUFFTs are of immediate interest for standard NFFF transformations [1].

In order to improve the antenna characterization results as compared to a standard transformation by exploiting the a priori information on the shape and size of the source [8, 9, 21], the aperture

field E_a is represented by the Prolate Spheroidal Wave Functions (PSWFs) as [9, 21–23]

$$E_a(x, y) = \sum_{r=1}^R \sum_{s=1}^S \alpha_{rs} \Phi_r [c_x, x] \Phi_s [c_y, y] \quad (5)$$

where $\Phi_i[c_w, w]$ is the i -th, 1D PSWF with “space-bandwidth product” c_w [22, 23], $c_x = au'$, $c_y = bv'$ and u' and v' locate the spectral region of interest [21], as $u' \leq \beta$ and $v' \leq \beta$. In Eq. (5), $R = \text{Int}[4a/\lambda]$ and $S = \text{Int}[4b/\lambda]$, $\text{Int}[x]$ denoting the integer part of x . Accordingly, once the PWS has been determined, it is filtered by calculating the aperture field E_a and by projecting it on the space of $R \times S$ PSWFs.

3. PHASELESS NUFF TRANSFORMATION

In the case of phaseless measurements, in order to restore the information lost due to the lack of the phase, the field amplitude is acquired, for example, on two different planes located at $d = z_1$ and $d = z_2$ [21, 24]. In the case of our interest, on both the domains, the acquisition is performed on a plane-polar geometry with $\Delta\rho_m$ and $\Delta\phi_m$ chosen so that the sampling step is $\lambda/4$ both radially and angularly.

Concerning the acquisition domains, in principle, they should change from one measurement plane to the other to account for the different truncation levels on the two planes. However, for the sake of simplicity, they will be kept the same in the following and indicated by the symbol D in both the cases. Furthermore, although the NUFFT technique can be applied to different kinds of phaseless approaches [21, 24, 25], in this paper we refer to the one in [21] which has been shown more effective than that in [24]. Nevertheless, the proposed calculation procedure applies also to the so-called “plane-to-plane” approach.

For the technique in [21], the aperture field is given again the expansion in Eq. (5) and the characterization of the antenna amounts at the determination of the aperture field E_a in terms of the α_{rs} 's and to the subsequent calculation of the FF pattern by minimizing the functional

$$\Phi(\underline{a}) = \sum_{i=1}^2 \frac{\|\tilde{M}_i^2(x, y) - |E_i(x, y; \underline{a})|^2\|_{\mathcal{L}^2(D)}}{\|\tilde{M}_i^2(x, y)\|_{\mathcal{L}^2(D)}} \quad (6)$$

where \tilde{M}_i^2 is the measured squared amplitude at the point (x_{mn}, y_{mn}) on the i -th surface, E_i is the complex field numerically predicted, at the generic iteration step, on the relevant plane-polar grid, \underline{a} is the

matrix collecting the unknown coefficients α_{rs} 's and $\|\cdot\|_{\mathcal{L}^2}$ is the usual L^2 norm.

At each iteration step, an estimate of \underline{a} is computed. From that, the aperture field and, thus, the PWS can be calculated. The evaluation of E_i on the plane-polar grid from the knowledge of the PWS can be performed as

$$E_i(x_k, y_k) = e^{-jw_{pq}z_i} \left(\frac{2\beta}{N}\right)^2 \sum_{p=-\frac{N}{2}}^{\frac{N}{2}} \sum_{q=-\frac{N}{2}}^{\frac{N}{2}} \hat{E}(u_p, v_q) e^{-j2\pi \left[\frac{p}{N} \left(\frac{2x_k}{\lambda} \right) + \frac{q}{N} \left(\frac{2y_k}{\lambda} \right) \right]}, \quad (7)$$

which is the expression of a 2D NER-NUDFT. Similarly, it can be seen that the evaluation of the functional gradient [21] requires the use of a 2D NED-NUDFT, so that the phaseless case requires the use of both, NER- and NED-NUFFT routines.

4. THE NUFFT ROUTINES

In order to shortly illustrate the NUFFT routines, we refer, for the sake of simplicity, to the 1D NER case. The corresponding NUDFT writes as

$$z_k = \sum_{p=-\frac{N}{2}}^{\frac{N}{2}} \hat{z}_p e^{-j2\pi x_k \frac{p}{N}}. \quad (8)$$

The main idea of the NUFFT algorithm is to approximate, following the Poisson formula, the “nonuniform” exponential $\exp(-j2\pi x_k p/N)$ by interpolating few, “oversampled”, “uniform” exponentials according to [16]

$$e^{-j2\pi x_k \frac{p}{N}} = \frac{(2\pi)^{-\frac{1}{2}}}{\Psi\left(\frac{2\pi p}{cN}\right)} \sum_m \hat{\Psi}(cx_k - m) e^{-j2\pi m \frac{p}{cN}}, \quad (9)$$

where $c > 1$ is an “oversampling” factor, Ψ , for example in the approach of [16], is the Kaiser-Bessel window, and $\hat{\Psi}$ is its Fourier transform.

By exploiting Eq. (9), Eq. (8) can be rewritten as

$$z_k = \frac{1}{\sqrt{2\pi}} \sum_m \hat{\Psi}(cx_k - m) \sum_{p=-\frac{N}{2}}^{\frac{N}{2}} \frac{\hat{z}_p}{\Psi\left(\frac{2\pi p}{cN}\right)} e^{-j2\pi m \frac{p}{cN}}. \quad (10)$$

Taking now into account that $\hat{\Psi}$ has finite support, then Eq. (10) takes the form

$$z_k = \sum_{m=-K}^K \hat{\Psi}(cx_k - m)U_{m+\mu_k}, \quad (11)$$

where K is typically 3 or 6 for single or double precision arithmetics, respectively, $\mu_k = \text{Int}[cx_k]$ and the subscript has to be considered cN -periodic.

Accordingly, the NUDFT can be effectively evaluated in three steps

(i) *Scaling and zero padding*

$$u_p = \begin{cases} 0 & p = -\frac{cN}{2}, \dots, -\frac{N}{2} - 1 \\ \frac{\hat{z}_p}{\Psi_p} & p = -\frac{N}{2}, \dots, \frac{N}{2} \\ 0 & p = \frac{N}{2} + 1, \dots, \frac{cN}{2} \end{cases}; \quad (12)$$

(ii) *FFT of $\{u_p\}_{p=-cN/2}^{cN/2}$ on cN points to obtain $\{U_k\}_{k=-cN/2}^{cN/2}$;*

(iii) *Cyclic convolution to calculate Eq. (10).*

It should be mentioned that this approach, for a fixed computational burden, proves to be more convenient than other interpolation+FFT based schemes [14,15] due to the use of the expansion in Eq. (9) purposely worked out for the exponentials involved in the NUDFT.

A similar procedure applies to the NED-NUFFT, but with steps (i) and (iii) exchanged.

5. NUMERICAL AND EXPERIMENTAL RESULTS

To illustrate the computational convenience and the accuracy of the procedure, we here present numerical and experimental results.

More in detail, the computational conveniences are first shown by numerical results obtained on an Intel Pentium D CPU 3.4 GHz, 4 GB of RAM, installed on an ASUSTek P5D DH Deluxe motherboard.

They aim at showing the better performance of both, 2D NED- and NER-NUFFT routines as compared to implementations of the 2D NED- and NER-NUDFT by optimized matrix-vector multiplications realized by the Basic Linear Algebra Subroutines (BLAS) as well as at proving the computational convenience against a NFFF transformation exploiting an Optimal Sampling Interpolation (OSI) step before a standard FFT as in [3, 12].

Table 1. Computational comparison between two versions of the complex NFFF transformation, one exploiting the OSI+FFT approach and one the proposed NUFFT-based technique.

Radius of D	OSI+FFT time [s]	NUFFT time [s]	Speedup
5λ	0.077	0.025	3.1
10λ	0.26	0.05	5.2
15λ	0.78	0.15	5.2

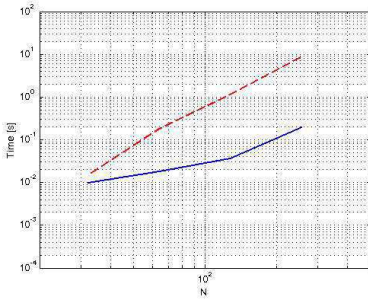


Figure 2. Blue solid line: execution times for the 2D NED-NUFFT. Red dashed line: execution times for the BLAS.

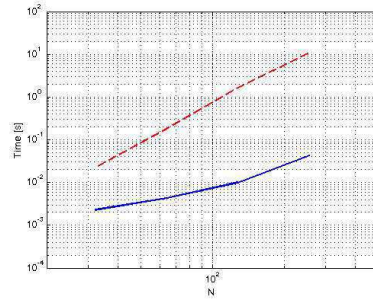


Figure 3. Blue solid line: execution times for the 2D NED-NUFFT. Red dashed line: execution times for the BLAS.

Furthermore, a test on experimental data collected at the Microwave and Millimeter Wave Laboratory, Dipartimento di Ingegneria Biomedica, Elettronica e delle Telecomunicazioni (DIBET), Università di Napoli Federico II, is illustrated.

The results regard a horn antenna (NARDA model No. 639), having an aperture of $57\text{ mm} \times 43\text{ mm}$, working in the Ku band, and characterized at 15 GHz from measurements performed on a planar scanning surface set at 6.5λ for the complex case and on two planar scanning surfaces set at 6.5λ and 14λ for the phaseless case. A domain D with radius equal to 15λ has been chosen in both the cases.

A further dataset with the usual, $\lambda/2$ step over a square Cartesian grid of $15\lambda \times 15\lambda$, set at a distance of 6.5λ from the aperture was also acquired to provide a reference for the results.

5.1. Computational Performance Results

In Table 1, the computation times for two versions of the complex NFFF transformation, one exploiting the OSI+FFT approach and one

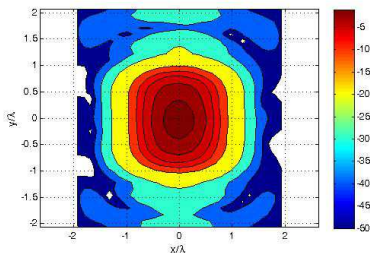


Figure 4. Amplitude of the aperture field recovered by the complex plane-polar NFFF transformation.

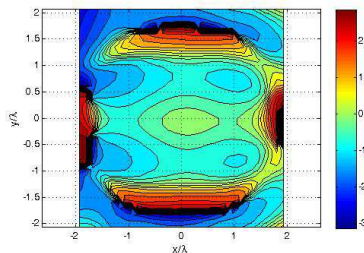


Figure 5. Phase of the aperture field recovered by the complex plane-polar NFFF transformation.

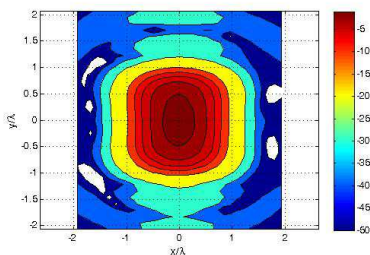


Figure 6. Amplitude of the reference aperture field.

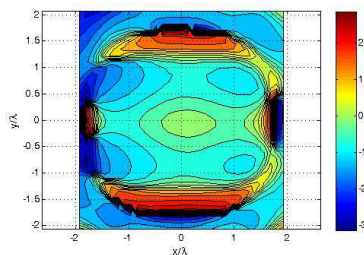


Figure 7. Phase of the reference aperture field.

the proposed NUFFT-based technique, are indicated for different sizes of the scanning plane. As it can be seen, the latter reaches relevant speedups as compared to the former.

Figures 2 and 3, on the other side, compare the computation times, for the 2D NED- and NER-NUDTFs, of the respective NUFFT implementations and the BLAS versions, against the size of the transform to be performed. The NUFFT results more convenient than the BLAS.

In all the considered cases, the computational times have been obtained by averaging 25 runs of each involved algorithm.

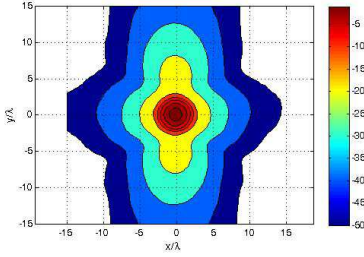


Figure 8. Amplitude of the field at 6.5λ recovered by the complex plane polar NFFF transformation.

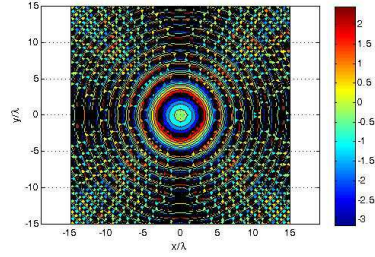


Figure 9. Phase of the field at 6.5λ recovered by the complex plane polar NFFF transformation.

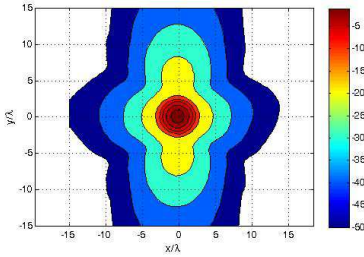


Figure 10. Amplitude of the reference field at 6.5λ .

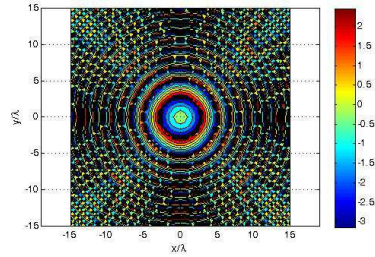


Figure 11. Phase of the reference field at 6.5λ .

5.2. Complex NFFF Transformation Results

Figures 4 and 5 illustrate the amplitude and phase, respectively, of the aperture field as retrieved by the NUFFT-based plane-polar NFFF transformation which compares satisfactorily with the reference depicted in Figures 6 and 7.

On the other side, Figures 8 and 9 illustrate the field reconstructed on the plane at $z = 6.5\lambda$ following the determination of the aperture field by the NUFFT-based NFFF transformation. Again, it compares satisfactorily with the reference one in Figures 10 and 11.

Finally, in Figures 12 and 13 we show the cuts, along the u and v axis, respectively, of the reference and reconstructed FFs. A very good agreement between the two results can be appreciated.

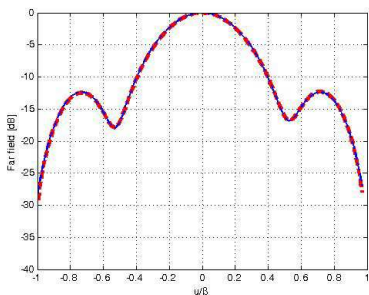


Figure 12. Blue solid line: cut along the u axis of the FF recovered by the complex plane polar NFFF transformation. Red dashed line: reference.

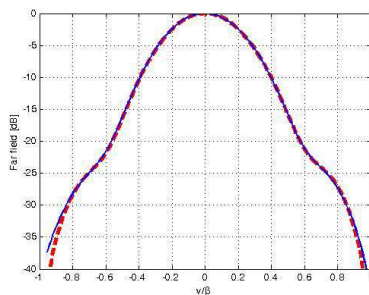


Figure 13. Blue solid line: cut along the v axis of the FF recovered by the complex plane polar NFFF transformation. Red dashed line: reference.

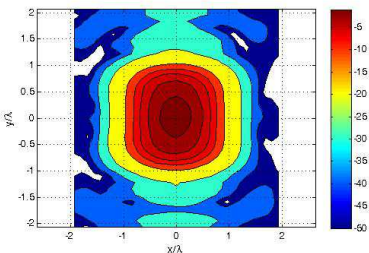


Figure 14. Amplitude of the aperture field recovered by the phaseless plane-polar NFFF transformation.

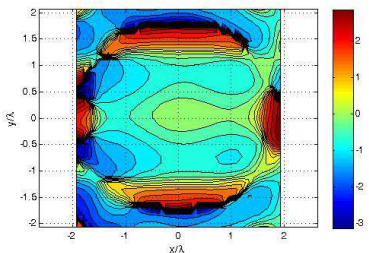


Figure 15. Phase of the aperture field recovered by the phaseless plane-polar NFFF transformation.

5.3. Phaseless NFFF Transformation Results

Concerning the phaseless case, in Figures 14 and 15, we show the amplitude and phase, respectively, of the aperture field reconstructed by the discussed algorithm. On the other side, in Figures 16 and 17, the amplitude and phase, respectively, of the field recovered on the surface at $z = 6.5\lambda$ and reconstructed by the phaseless approach are displayed. Those two results compare well again with the reference ones in Figures 6 and 7 and Figures 10 and 11, respectively.

Similarly, in Figures 18 and 19 we show the cuts, along the u and v axis, respectively, of the reference and reconstructed FFs. A very

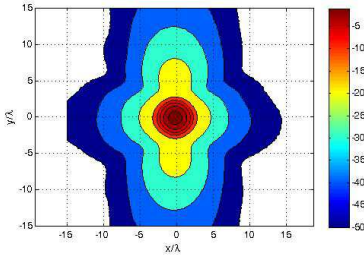


Figure 16. Amplitude of the field at 6.5λ recovered by the phaseless plane polar NFFF transformation.

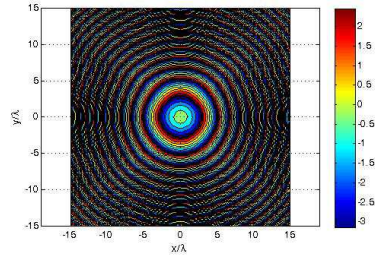


Figure 17. Phase of the field at 6.5λ recovered by the phaseless plane polar NFFF transformation.

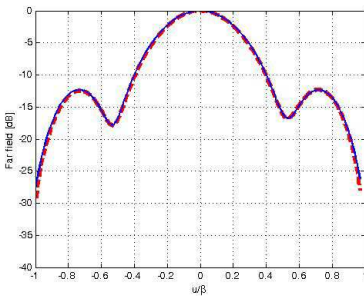


Figure 18. Blue solid line: cut along the u axis of the FF recovered by the phaseless plane polar NFFF transformation. Red dashed line: reference.

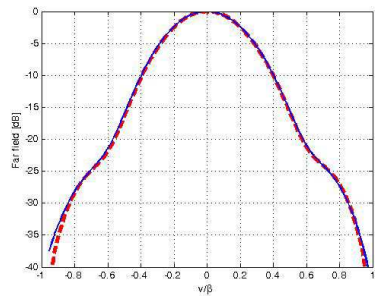


Figure 19. Blue solid line: cut along the v axis of the FF recovered by the phaseless plane polar NFFF transformation. Red dashed line: reference.

good agreement between the two results can be again appreciated, showing that the phaseless approach is capable to achieve successful characterizations also in the case of non-focusing antennas.

6. CONCLUSIONS

We have introduced the use of Non-Uniform Fast Fourier Transform (NUFFT) routines in “complex” (i.e., amplitude and phase) and phaseless Near-Field/Far-Field transformations. In the considered case of a plane-polar acquisition geometry, the use of those routines

results computationally much more convenient when non-regular field sampling prevents the use of standard FFTs as compared to other schemes (e.g., using BLAS routines or OSI interpolation+FFT), as shown by the numerical analysis. The experimental results have proven the satisfactory accuracy of the technique.

In conclusion, the proposed technique makes available an approach, given NUFFT routines, enabling a simple and convenient NFFF transformation also in the case on non-regular sampling grids.

REFERENCES

1. Yaghjian, A., "An overview of near-field antenna measurements," *IEEE Trans. Antennas Propag.*, Vol. 34, No. 1, 30–45, Jan. 1986.
2. Bucci, O. M., C. Gennarelli, and C. Savarese, "Representation of electromagnetic fields over arbitrary surfaces by a finite and nonredundant number of samples," *IEEE Trans. Antennas Propag.*, Vol. 46, No. 3, 351–359, Mar. 1998.
3. Bucci, O. M., C. Gennarelli, and C. Savarese, "Fast and accurate near-field-far-field transformation by sampling interpolation of plane-polar measurements," *IEEE Trans. Antennas Propag.*, Vol. 39, No. 1, 48–55, Jan. 1991.
4. D'Agostino, F., F. Ferrara, C. Gennarelli, R. Guerriero, and M. Migliozi, "Near-field-far-field transformation technique with helicoidal scanning for elongated antennas," *Progress In Electromagnetics Research B*, Vol. 4, 249–261, 2008.
5. Ferrara, F., C. Gennarelli, R. Guerriero, R. Riccio, and C. Savarese, "An efficient near-field to far-field transformation using the planar wide-mesh scanning," *Journal of Electromagnetic Waves and Applications*, Vol. 21, No. 3, 341–357, 2007.
6. D'Agostino, F., C. Gennarelli, G. Riccio, and C. Savarese, "Theoretical foundations of near-field-far-field transformations with spiral scannings," *Progress In Electromagnetics Research*, Vol. 61, 193–214, 2006.
7. Qureshi, M. A., C. H. Schmidt, and T. F. Eibert, "Adaptive sampling in multilevel plane wave based near-field far-field transformed planar near-field measurements," *Progress In Electromagnetics Research*, Vol. 126, 481–497, 2012.
8. Capozzoli, A., C. Curcio, A. Liseno, and P. Vinetti, "Field sampling and field reconstruction: A new perspective," *Radio Sci.*, Vol. 45, RS6004, 31, 2010, doi: 10.1029/2009RS004298.
9. Capozzoli, A., C. Curcio, G. D'Elia, and A. Liseno, "Singular-value optimization in plane-polar near-field antenna characteri-

- zation,” *IEEE Antennas Prop. Mag.*, Vol. 52, No. 2, 103–112, Apr. 2010.
10. Capozzoli, A., C. Curcio, and A. Liseno, “Multi-frequency, multi-resolution and probe compensated advanced near-field antenna characterization,” *Proc. of the Europ. Conf. on Antennas Prop.*, 2542–2546, Prague, Czech Republic, Mar. 26–30, 2012.
 11. Gatti, M. S. and Y. Rahmat-Samii, “FFT applications to plane-polar near-field antenna measurements,” *IEEE Trans. Antennas Propag.*, Vol. 36, No. 6, 781–791, Jun. 1988.
 12. Yaccarino, R. G., Y. Rahmat-Samii, and L. I. Williams, “The bipolar planar near-field measurement technique, Part II: Near-field to far-field transformation and holographic imaging methods,” *IEEE Trans. Antennas Propag.*, Vol. 42, No. 2, 196–204, Feb. 1994.
 13. Capozzoli, A., C. Curcio, G. D’Elia, A. Liseno, and P. Vinetti, “Fast CPU/GPU pattern evaluation of irregular arrays,” *Applied Comput. Electromagn. Soc. J.*, Vol. 25, No. 4, 355–372, Apr. 2010.
 14. Capozzoli, A., C. Curcio, A. Liseno, and P. Vinetti, “Fast interpolation accelerated on GPU for SAR backprojection,” *Proc. of the 27th Annual Rev. of Progr. in Appl. Comput. Electromagn.*, 1–6, Columbus, OH, Apr. 10–14, 2012.
 15. Capozzoli, A., C. Curcio, and A. Liseno, “Fast GPU-based interpolation for SAR Backprojection,” *Progress In Electromagnetics Research*, Vol. 133, 259–283, 2013.
 16. Fourmont, K., “Non-equispaced fast Fourier transforms with applications to tomography,” *J. Fourier Anal. Appl.*, Vol. 9, No. 5, 431–450, Sep. 2003.
 17. Greengard, L. and J.-Y. Lee, “Accelerating the nonuniform fast Fourier transform,” *SIAM Review*, Vol. 46, No. 3, 443–454, Sep. 2004.
 18. Lee, J.-Y. and L. Greengard, “The type 3 nonuniform FFT and its applications,” *J. Comput. Phys.*, Vol. 206, No. 1, 1–5, Jun. 2005.
 19. Capozzoli, A., C. Curcio, and A. Liseno, “GPU-based ω - k tomographic processing by 1D non-uniform FFTs,” *Progress In Electromagnetics Research B*, Vol. 23, 279–298, 2012.
 20. Rahmat-Samii, Y., V. Galindo-Israel, and R. Mittra, “A plane-polar approach for far-field construction from near-field measurements,” *IEEE Trans. Antennas Propag.*, Vol. 28, No. 2, 216–230, Mar. 1980.
 21. Capozzoli, A., C. Curcio, G. D’Elia, and A. Liseno, “Phaseless antenna characterization by effective aperture field and data

- representations," *IEEE Trans. Antennas Propag.*, Vol. 57, No. 1, 215–230, Jan. 2009.
22. Landau, H. J. and H. O. Pollak, "Prolate spheroidal wave functions, Fourier analysis and uncertainty — III: The dimension of essentially time- and band-limited signals," *Bell Syst. Tech. J.*, Vol. 41, 1295–1336, Jul. 1962.
 23. Frieden, B. R., "Evaluation, design and extrapolation methods for optical signals, based on use of the prolate functions," *Progress in Optics*, Vol. 9, 311–407, E. Wolf, Ed., North-Holland, Amsterdam, 1971.
 24. Yaccarino, R. G. and Y. Rahmat-Samii, "Phaseless bi-polar planar near-field measurements and diagnostics of array antennas," *IEEE Trans. Antennas Propag.*, Vol. 47, No. 3, 574–583, Mar. 1999.
 25. Ribière-Tharaud, N., M. Lambert, and P. Levesque, "Wideband validation of a phase retrieval process applied to infrared planar near-field measurements," *Progress In Electromagnetics Research B*, Vol. 23, 39–54, Jan. 2010.